International Journal of Adhesion & Adhesives 31 (2011) 550–558

Contents lists available at ScienceDirect

International Journal of Adhesion & Adhesives

journal homepage: www.elsevier.com/locate/ijadhadh

Shear decohesion of clamped abraded steel interfaces reinforced with epoxy adhesive

A. Oinonen *, G. Marquis

Aalto University School of Science and Technology, Department of Applied Mechanics, P.O. Box 14300, FIN-00076 Aalto (Espoo), Finland

ARTICLE INFO

Article history:
Accepted 6 May 2011
Available online 17 May 2011

Keywords:
Cohesion
Epoxides
Fracture
R-curves
Surface roughness

ABSTRACT

This paper presents an experimental assessment of quasi-static shear strength of the combined mechanically clamped and epoxy adhesive reinforced steel interfaces. The effect of the surface roughness and clamping load on the combined interfacial decohesion and slipping is investigated. The maximum shear strength of the adhesive reinforced specimens with fine ground, coarse ground and grit blasted contact surface finishes is reported with comparison to the results of the identical non-reinforced specimens. Results have been assessed both in terms of calculated fracture energy and interface decohesion. The bonded interfaces with grit blasted finish showed considerably higher maximum shear stresses as compared to the identical ground cases. The shear strength contributions of strong clamping and reinforcing conformed well to the principle of superposition for all experimented interface types.

1. Introduction

Joining of structural members by adhesive bonding has been motivated by the desire to improve the fatigue strength of traditional bolted or welded connections and to prevent structural distortion due to the welding process [1]. In order to improve static strength, slip resistant bolted joints in steel with adhesive reinforced lap interfaces have been introduced by Albrecht and Sahli [2]. For example, in highway bridge applications reinforcement bonding is made using two component epoxy [3] or acrylic [2] adhesives with high elastic modulus. For reinforced frictional connections, mechanical fastening provides high slip-resistance in shear (mode II) and helps to prevent peeling (mode I) failures of the adhesive. The internal strength, i.e. cohesion, of the hardened adhesive material increases the maximum shear strength of the joint interface. Furthermore, the relatively low Young's modulus of the adhesive increases local flexibility of the mechanically connected interface and thus reduces stress concentration between the higher modulus adherents fabricated from steel.

Dragoni and Mauri [4,5] and Sawa et al. [6] have investigated the maximum shear strength of reinforced clamped interfaces using annular-type specimens, which were subject to torsion loading. Tests involving ground contact surfaces and strong anaerobic adhesives (retainers) [4] have shown that the friction force is linearly dependent on the applied clamping pressure and that the adhesive provides a constant peak value in mean shear strength, which is independent from the applied axial clamping stress [4–6]. Therefore, the combined slipping and interface damage based shear load vs. displacement response of adhesively retained joints can be characterized based on the principle of superposition. However, the experiments on adhesives with lower strength [5] have shown that the superposition method cannot be adapted as a general rule. Consequently, further studies concerned with interfaces in high strength steel (HSS) involving the combination of the two component epoxy adhesive with high elastic modulus and considerably rougher surface finish are needed.

During the assembly process of adhesively reinforced joints with adherents in steel, the fasteners are tightened before the adhesive is cured [2,4–6]. In such a case, the normal pressure between the plates created by the fasteners is high enough to force uncured adhesive out from the interface region and only small quantities remain to fill in the micro-volumes between the contact surfaces [4,5]. Obviously, the resulting elastic–plastic deformation of the original interface topography due to clamping is dependent on the initial surface roughness and yield limit of the adherent material. Thus, only a part of the adherent surfaces is in contact with the adhesive and metal-to-metal contact will occur adjacent to the formed micro-cavities. Therefore, an adhesive layer with a constant thickness, as is sometimes observed in adhesive joints with lower clamping stress, does not provide an accurate physical assumption for reinforced joints in HSS involving high clamping stress.

The effects of curing temperature on the shear strength of the adhesively bonded lap-joints have been investigated by Matsui [7].

* Corresponding author. Tel.: +358947023443; fax: +358947023449.
E-mail addresses: ahti.oinonen@aalto.fi (A. Oinonen), gary.marquis@aalto.fi (G. Marquis).

0143-7496/$ - see front matter © 2011 Elsevier Ltd. All rights reserved.
doi:10.1016/j.ijadhadh.2011.05.002

Nomenclature

i	index defining the mode (I, II, III) of the load or degradation
q	uniform normal pressure at the interface due to the preload
t_i	traction stress at the contact interface
t_i^c	maximum value of the traction stress at the cohesion interface
t_i^r	residual traction stress at the fully damaged interface due to sliding friction
A	pre-stress dependency slope
B	pre-stress independent portion of the interfacial shear stress
α	non-dimensional decay exponent (interface material parameter)
δ_i	relative displacement at the cohesion interface
δ_i^c	critical relative displacement corresponding to the peak shear stress
δ_i^f	relative displacement corresponding to the fully degraded interface
κ_i	stiffness of the contact interface
τ_{II}	measured total shear stress at the contact interface
τ_{II}^p	measured maximum value of the total shear stress
Δ	measured relative displacement due to applied shear load
Δ^c	measured critical relative displacement at the beginning of the slip
G_i	fracture energy release rate of the reinforced interface
G_i^c	critical fracture energy release rate

For heat-cured epoxy adhesive joints, the results indicated a substantial increase in the average ultimate shear stress as compared to existing data from similar specimens cured at room temperature. Stewart et al. [8] have also reported a notable increase in the lap shear strength of the epoxy adhesive joints, which had underwent 4 h post curing in 40–90 °C.

The shear load carrying capacity of thermosetting epoxy adhesives has been observed to increase when the adhesive thickness is decreased [9,10]. Consequently, the critical fracture energy of the adhesive material has been shown to strongly decrease if the thickness of the adhesive layer is increased [10]. Furthermore, the relationship between shear strength and surface roughness shows only a marginal of 3 MPa decrease in the maximum shear stress of the epoxy bonded lap-joint when the arithmetical mean roughness, *Ra*, of the surface is increased from 1 to 3 μm [11]. It has been concluded that the dependency between joint strength and surface finish is a complex phenomenon and cannot be generalized for different loading conditions and materials involved [9,12].

Typically, the shear deformation and fracture of structural adhesives are assessed using the Napkin Ring specimens [13]. This testing procedure consists of applying equal and opposite torque to two tubular adherents butt joined by adhesive [13]. The method produces a relatively uniform shear stress distribution within the adhesive due to the continuous surface and small difference between the inner and outer diameter of the specimen [14]. Moreover, the axial clamping load can be applied to the interface without disturbing the shear stress uniformity.

Recently, damage mechanics based cohesive zone models (CZMs) [15,16] have been adapted to model decohesion of adhesively bonded interfaces involving clamping pressure [17,18]. Oinonen and Marquis [18] have developed a modeling procedure that includes both the cohesive and frictional properties at the clamped joint interface. Different formulations for CZM are exploited to model the normal and shear tractions vs. relative displacement responses between the adherents [15–19]. The suggested CZM is particularly suitable for the applications where significant clamping pressures are involved, e.g. reinforced non-slip bolted joints. An experimentally validated CZM can be implemented in the selected finite element analysis programs and thus provide a versatile modeling approach for the more complex adhesive joining related engineering problems [17–19].

During decohesive cracking, fracture energy is dissipated. For ductile and semi-ductile materials, resistance to fracture material bonds and displacement of the fracture surfaces is often described using *R*-curves, i.e. energy dissipation as a function of the extent of crack propagation [20]. Previously, the *R*-curve has been used to describe the fracture resistance of bonded [19] and adhesively reinforced frictional joints [18]. Particularly for reinforced interfaces, the contribution of sliding frictional dissipation is excluded from the *R*-curve [18]. In general, the *R*-curve should be determined directly from the actual energy release rate. The *R*-curve should not be used for fully brittle fracture [21]. In the cases involving unavoidable non-steady crack propagation due to a periodically brittle interface fracture, the effective *R*-curve term can be used [22]. A consistently determined R_{eff}-curve can be regarded as a mechanical interface property and it additionally provides an appropriate theoretical connection with the corresponding CZM [22].

This paper is concerned with the detailed experimental assessment of mode II decohesion of the combined clamped and adhesively reinforced interfaces. With structural applications in mind, a two component epoxy adhesive with the high stiffness and good resistance to increased ambient temperatures was used for reinforcing the HSS specimens. The influence of combined decohesion of heat-cured epoxy and abraded HSS under significant clamping pressure on the mode II strength vs. relative displacement response is investigated. Peak values of the measured mode II stress at the interfaces are reported. Results obtained from specimens with highly abraded (grit blasted) contact surfaces are compared with the identical loading cases involving the considerably smoother (ground) contact surfaces. The observed mode II fracture behavior, i.e. brittle, semi-brittle or ductile, under different clamping pressure and abrasion conditions is assessed. When applicable, the R_{eff}-curves are integrated. For reference, peak shear stress values obtained from non-bonded specimens with identical surface finishes and clamping pressure are presented. The CZM developed in a previous work [18] was parametrically fitted for the epoxy reinforced grit blasted interfaces. The fracture assessment reported in the current paper can be assumed to provide an input for design data and improve a modeling accuracy of both the reinforced and non-bonded frictional HSS interfaces with different surface roughness.

2. Shear decohesion model

The reinforced interface consists of the pre-stressed HSS surface inter-contact and adhesive material, which is contained primarily with micro-volumes created by the surface roughness. In general, CZM is based on the traction vs. separation response for each mode of loading (i=I, II, III). For a clamped joint, the

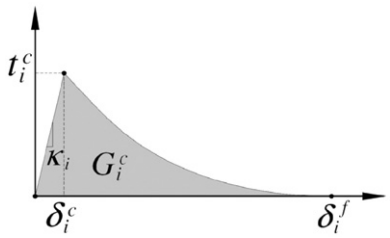

Fig. 1. Linear-exponential CZM of the reinforced interface. The critical fracture energy release rate G_i^c is defined as a value of the area integral.

shear mode is assumed to be exclusively active at the interface, i.e. mode II for two-dimensional (2D) cases and correspondingly modes II and III for 3D. For strong adhesives [4,5], the steady frictional stress contribution can be excluded from CZM based on the principle of superposition [18]. With reference to the experimental data reported in Section 4.2, the progressive damage of the epoxy reinforced interface can be characterized as the linear-exponential CZM shown in Fig. 1.

With reference to Fig. 1, the interface stiffness parameter κ_i determines the linear-elastic slope of the deformation response across the interface. The decohesive degradation initiates when the maximum interface traction stress t_i^c is reached corresponding to the critical relative displacement between the surfaces δ_i^c. As δ_i further increases, t_i exponentially decays until the full damage has been accumulated corresponding to a zero residual of t_i. The non-linear part of the linear-exponential decohesion evolution law is formulated as the exponential function. Finally, CZM can be expressed as

$$t_i(\delta_i) = \begin{cases} \kappa_i \delta_i, & 0 < \delta_i \le \delta_i^c \\ t_i^c \exp[\alpha(\delta_i - \delta_i^c)] & \delta_i^c < \delta_i \le \delta_i^f \end{cases}, \quad (1)$$

where α is the non-dimensional decay exponent. The critical fracture energy release rate G_i^c for each mode is defined as the work done by t_i corresponding to the respective δ_i. The numerical value of G_i^c can be obtained by integrating t_i vs. δ_i response [20,23]

$$G_i^c = \int_0^{\delta_i^f} t_i(\delta_i) d\delta_i. \quad (2)$$

3. Experimental assessment

An experimental program was initiated to determine the interface shear stress vs. relative displacement curves for both the reinforced and non-bonded specimens. The effect of the clamping load and surface roughness on the maximum mode II decohesive dissipation was investigated. Five different axial pre-load values, $q \in [4,50,100,150,200]$ MPa, were considered for each surface finish variation. The value $q=4$ MPa corresponded to the lowest pressure needed to force uncured adhesive out from the interface region and to firmly close the contact.

3.1. Specimens

Test specimens were machined from HSS sheets with a nominal yield strength 960 MPa. The design and dimensional details of the specimen are given in Fig. 2. All circular contact surfaces were cleaned with pure acetone to ensure the proper adhesion. The surfaces inside of the $\phi=56$ mm contact area were protected using an o-ring seal to prevent adhesion inside the desired contact areas and to reduce the build up of an inner spew fillet. During the assembly process, adhesive was exclusively applied to the contact surfaces of the specimens and clamping

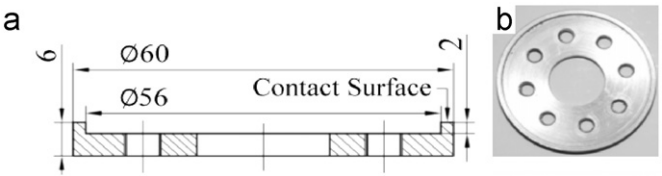

Fig. 2. (a) Test specimen with the main dimensions (mm) and (b) photograph of the specimen.

Table 1
Reported material properties of the structural epoxy adhesive DP760 based on the test method EN 2243-1 [24].

Young's modulus in 23 ± 2 °C	Shear limit—cured at 23 ± 2 °C	Shear limit—cured at 65 ± 3 °C
5972 MPa	28.2 MPa	29.1 MPa

Table 2
Measured contact surface roughness (μm).

Surface type	*Ra*	*Rz*	*Ry*
Fine ground	0.38	2.02	3.42
Coarse ground	0.57	3.26	5.34
Grit (aluminum oxide) blasted	3.57	22.42	31.21

to the desired pre-stress was immediately applied. The outer surfaces of the specimens were cleaned of excess uncured adhesive. The pre-defined clamping stress was constant during the curing process and it was not released before the subsequent testing was performed with the same stress. A two component structural epoxy adhesive DP760 [24] was used. Curing was performed at 65 ± 3 °C for 2 h [24]. Heat up time from 20 to 65 °C was 2½ h. For reference, the mechanical properties of the epoxy adhesive reported by the manufacturer are given in Table 1. In contrast to the present study, the limit stress data presented in Table 1 is based on overlap shear specimens in aluminum and 150 μm glue line thickness.

In the current work, grit blasted, coarse ground and fine ground contact surfaces were investigated. Surface roughness following abrading was measured in the circumferential direction from the sixteen randomly selected locations for each surface type. The measuring length of each measurement was 2.5 mm. The average arithmetical mean roughness (*Ra*), maximum peak (*Ry*) and ten-point mean roughness (*Rz*) are presented in Table 2. An example of the typical profile of the grit blasted contact surface is shown in Fig. 3.

The bond lines of the contact interfaces are shown in Fig. 4 for each surface type. These micro-sections were produced following the same gluing procedure as previously described. The constant pre-stress $q=100$ MPa was developed using an instrumented bolt and the pre-stress remained constant during curing, preparation and microscopic examination of the micro-section. For each bonded and clamped specimen pair, approximately 1 mm of material was machined away from the outer diameter. This new surface was then polished followed by microscopic examination.

3.2. Testing system

A schematic of the testing device used in this study is shown in Fig. 5. The servo-hydraulic actuated test machine applied pure torsion load across the circular specimen-pair interface. During testing, normal stress on the interfaces was maintained via a threaded rod equipped with an in-line axial load cell. The normal

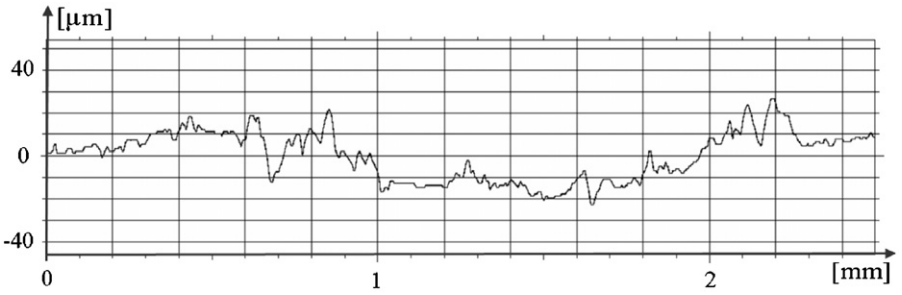

Fig. 3. Typical surface profile vs. measuring distance (2.5 mm) of the grit blasted surface before the clamping and testing procedure (produced using the TalyProfile 3.2.0 program).

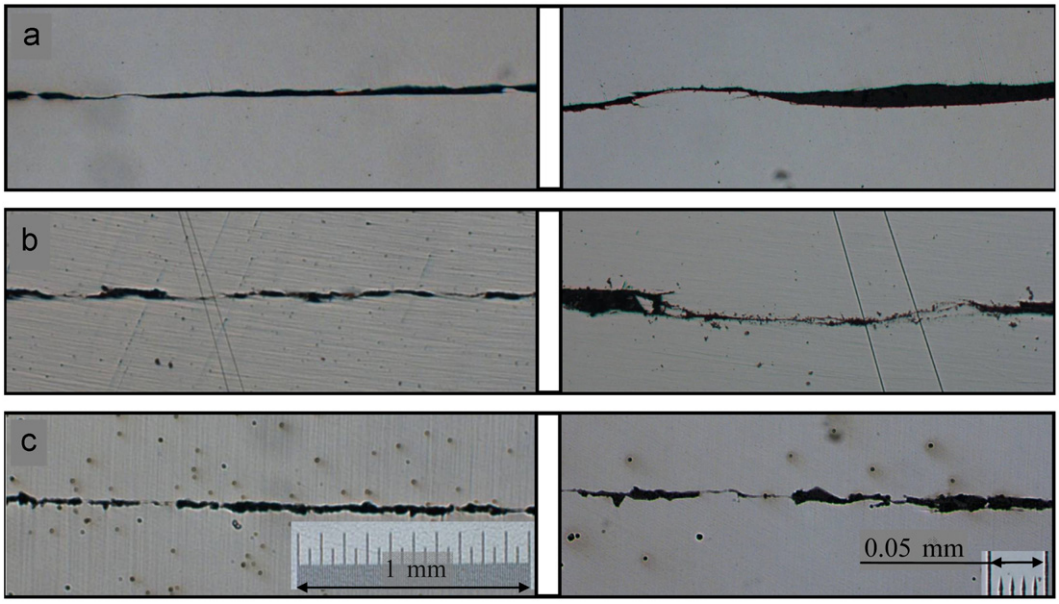

Fig. 4. Polished micro-sections of the tangential bond line of the contact interfaces under the clamping load $q=100$ MPa. The magnified details from the left figures are shown on the right for each interface type. (a) Fine ground, (b) coarse ground and (c) grit blasted.

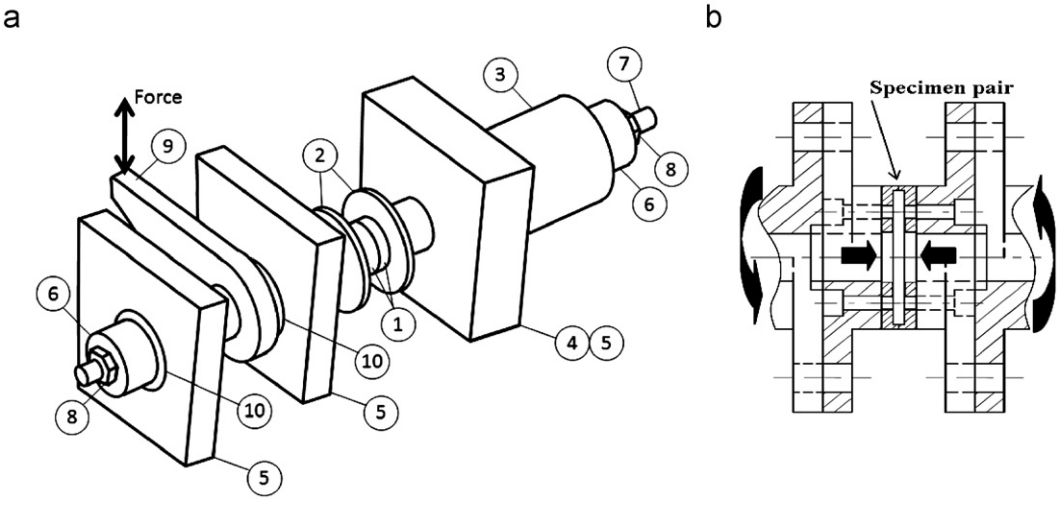

Fig. 5. (a) Schematic of the testing device. Key components are: (1) specimen pair, (2) specimen holders, (3) axial load cell, (4) torque reaction, (5) support, (6) thrust bearing, (7) threaded rod, (8) nut, (9) torque arm and (10) rotation bearing. (b) Detailed sketch with the applied direct and torsional loads.

stress was continuously measured during curing and testing in order to verify that it varied by no more than 1% from the desired value. The threaded rod was equipped with the low friction axial thrust bearings at each end. The influence of bearing friction due to preload on the measured torque was less than 1.5% for all tests. Therefore, the measured torque was assumed to be exclusively

transmitted across the interface. An eddy current extensometer was fixed to each side of the specimen pairs in order to measure displacement between the contact surfaces. The static resolution and measurement precision of the eddy current sensor were better than 10.0 and 20 μm, respectively. Rotation displacement was applied at the nominal rate of 0.027 mm/s measured at the mean diameter of the contact interfaces. During testing the temperature was maintained at 20 ± 1 °C.

4. Results

In this section, the maximum values of the total interface shear stress τ_{II}^p are presented for different cases of the normal pressure q. In addition, the τ_{II} vs. relative displacement Δ curves are plotted for the selected experiments. Based on experimentally observed decohesion response, the parameters of CZM are fitted for the grit blasted case. The R_{eff}-curves are produced to represent the development of the mode II energy release rate, G_{II} vs. Δ. For $1.0 < \Delta < 3.0$ mm, the responses of all bonded interfaces were observed to exclusively consist of sliding friction. Therefore, the range $0 \le \Delta \le 1.0$ mm was considered to be of primary interest for representing the result data. Finally, photographs of the fracture surfaces of the damaged interfaces for $q=4$ and 100 MPa are presented.

4.1. Peak values of interface shear stress

The measured peak values of the total shear mode stress τ_{II}^p vs. pre-stress q, is summarized in Fig. 6. With reference to the τ_{II} vs. Δ responses shown in Figs. 7 and 8, the data points presented in Fig. 6 correspond to the observed $\tau_{II}^p(q)$. This always occurred within the displacement range of $0 < \Delta < 0.15$ mm. Fig. 6 includes results from the studied surface finish variations both with and without bonding involving the significant pre-stress, i.e. $q \in [50,200]$ MPa. For the experiments involving the non-bonded ground contact surfaces, non-linear slip hardening of the interfaces was observed as seen in Fig. 13. In such cases $\tau_{II}^p(\Delta^c)$ was assumed to correspond to the peak value at the beginning of the observed initial slip.

The linear least-squares fitting method [25] was applied to develop the relationship between τ_{II}^p and q

$$\tau_{II}^p(q) = Aq + B. \tag{3}$$

Eq. (3) provides an estimate for assessing $\tau_{II}^p(q)$ within the range of $q \in [50,200]$ MPa. The calculated fitting coefficients A and B for each interface variation are provided in Table 3. For $q=4$ MPa, a different failure mechanism was observed (see Section 4.2) and therefore, the data for $q=4$ MPa was excluded

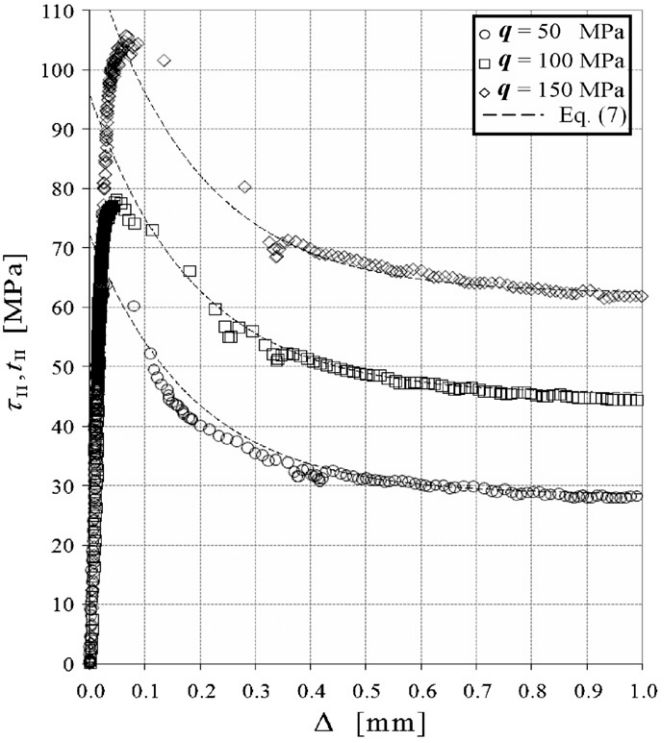

Fig. 7. Combined slip and interface decohesion responses of the specimens with the grit blasted contact surface finish. The test data of the conservative results $\tau_{II}(\Delta)$ is compared to the fitted exponential decay model, Eq. (7).

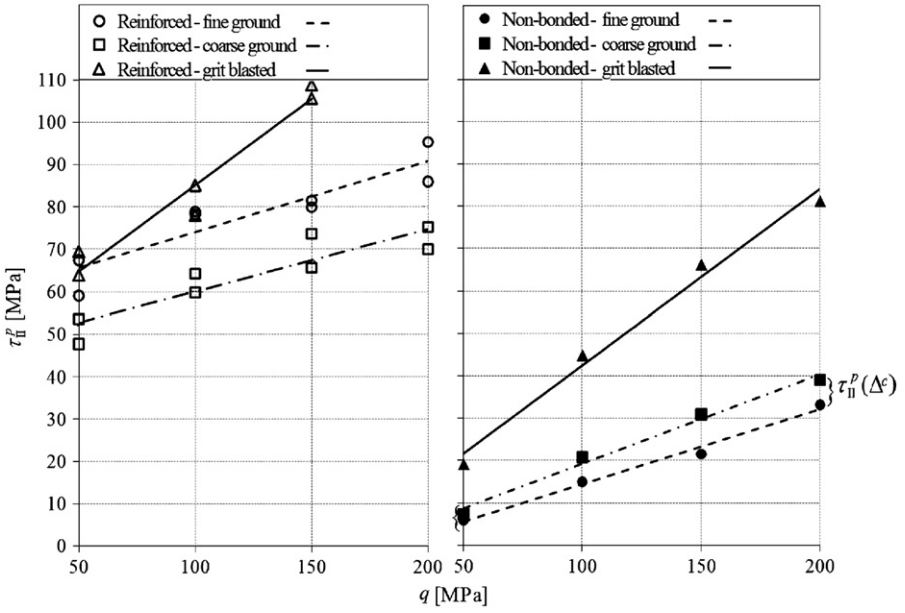

Fig. 6. Peak values of the measured interface shear stress τ_{II}^p vs. clamping stress q are shown with the corresponding linear least-squares fit. Exclusively for the non-bonded ground contact surfaces, $\tau_{II}^p(\Delta^c)$ corresponds to the peak value at the beginning of the observed initial slip.

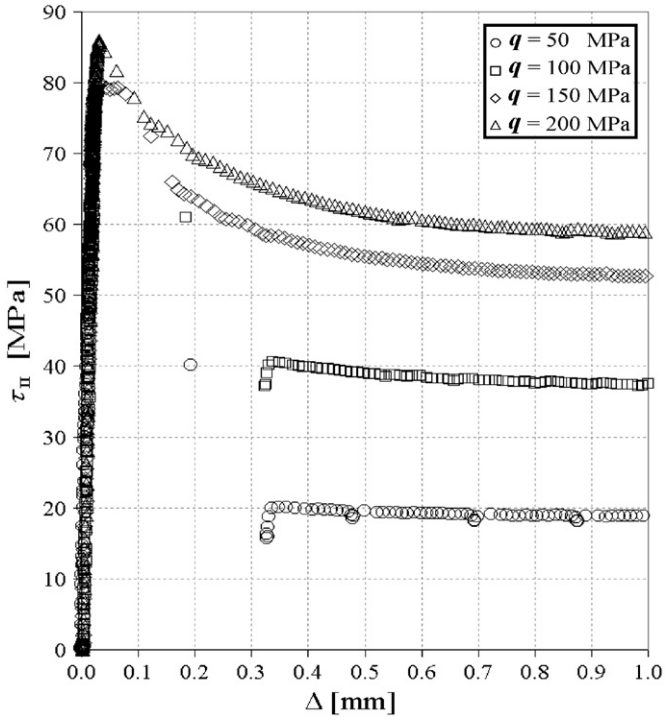

Fig. 8. Combined slip and interfacial decohesion responses of the specimens with the fine ground contact surface finish.

Table 3
Matrix of experiments and the numerical values of the fitting parameters for Eq. (3).

Interface type	Number of tests for each q	A	B
Fine ground—bonded	2	0.169	57.23
Fine ground—non-bonded	1	0.177	−3.21
Coarse ground—bonded	2	0.147	45.35
Coarse ground—non-bonded	1	0.211	−1.81
Grit blasted—bonded	2	0.406	44.56
Grit blasted—non-bonded	1	0.415	0.99

Table 4
Measured peak values of the interface shear stress τ_{II}^{p} for the low pre-stress $q=4$ MPa.

Interface type	τ_{II}^{p}, test I	τ_{II}^{p}, test II	Averageτ_{II}^{p} based on the tests I and II
Fine ground	49.43	46.21	47.82
Coarse ground	49.22	43.40	46.31
Grit blasted	54.51	52.08	53.30

from the regression fit. Peak shear stress values for this case are given in Table 4.

4.2. Decohesion response of reinforced interfaces

Fig. 7 shows the measured shear stress τ_{II} vs. displacement Δ response of the bonded specimens with the grit blasted contact surface finish. Two tests were performed for each pre-stress q and the data shown in Fig. 7 corresponds to the more conservative, i.e. lower τ_{II}^{p}, from the two identical experiments. The measured data for $q=200$ MPa is excluded from Fig. 7 due to observed incoherent and highly unstable response before attaining τ_{II}^{p} in two identically performed tests.

The interface stiffness parameter $\kappa_{II}\approx 3000\ \mathrm{N/mm^3}$ was approximated based on the experimental data. With reference to Fig. 1 and Eq. (1), the numerical values of the critical relative displacements can then be calculated from

$$\delta_{II}^{c}=t_{II}^{c}/\kappa_{II}. \tag{4}$$

The Curve Fitting Toolbox included in the MATLAB® [25] was applied for the fitting procedure of the non-linear part of Eq. (1). In cases where replicate experiments were performed, the more conservative result was used in fitting of CZM. The decay exponent of Eq. (1), $\alpha\approx -5.33$ was obtained by calculating an average of the different values of α for each q based on the original test data. In addition, the functions for the cohesive peak stress $t_{II}^{c}(q)$ and steady friction stress $t_{II}^{r}(q)$ could be developed by applying the linear least-squares method. By defining a common α and developing Eqs. (5) and (6), the number of parameters is decreased. This increase an applicability of the suggested decohesion model for engineering purposes. Finally, these equations can be combined with Eq. (1) to give the CZM part of Eq. (7). The resulting total response model, Eq. (7), is defined as a combination of the terms, which are linear in $t_{II}^{c}(q)$, $t_{II}^{r}(q)$ and non-linear in α for the selected pre-stress q. Fig. 7 shows the measured decohesion decay data for grit blasted specimens for three values of q. The figure also shows the corresponding fits calculated from Eq. (7) for $q\in[50,150]$ MPa.

$$t_{II}^{c}(q)=0.067q+33.09,\quad q\in[50,150]. \tag{5}$$

$$t_{II}^{r}(q)=0.34q+11.47,\quad q\in[50,150]. \tag{6}$$

$$t_{II}(\delta_{II},q)=t_{II}^{c}(q)\exp[-5.33(\delta_{II}-\delta_{II}^{c})]+t_{II}^{r}(q),\quad \delta_{II}\in[\delta_{II}^{c},\infty). \tag{7}$$

In Fig. 8, the combined slip and interface decohesion response of the specimens with the fine ground contact surface finish is shown. As with Fig. 7, only the more conservative, i.e. lower τ_{II}^{p}, data is shown from cases where replicate tests were performed. In addition, the resulting interface decohesion response of the coarse ground specimens for $0.0\le\Delta\le 0.1$ mm based on the experiments with $q=150$ and 200 MPa is shown in Fig. 9. Fig. 10 shows the contact surfaces for $q=4$ and 100 MPa after shear testing.

4.3. Effective R-curves of reinforced interfaces

The energy release rate G_{II} vs. relative displacement Δ, i.e. R_{eff}-curves of the reinforced interfaces, are shown in Fig. 11 for the grit blasted surface finish. These R_{eff}-curves were numerically integrated based on the original test data points. For all cases, G_{II} has reached approximately constant values at $\Delta=1.0$ mm. This is defined as G_{II}^{c}. With reference to CZM shown in Fig. 1 involving G_{II}^{c} defined by Eq. (8), the R_{eff}-curves exclusively include damage dissipation of the reinforced interface and the contribution of steady frictional dissipation is excluded [18]. The cases involving the predominantly brittle or unstable decohesion fracture were considered as non-relevant sources and the respective R_{eff}-curves could not be developed.

$$G_{II}^{c}=\int_{0}^{1.0}[\tau_{II}(\Delta)-\tau_{II}(1.0)]d\Delta. \tag{8}$$

4.4. Decohesion of non-reinforced interfaces

The combined slip and pure HSS decohesion responses of the specimens without adhesive reinforcement were also experimentally measured. This data is necessary in order to assess the adhesive's influence on the shear strength of the interface. The plot presenting τ_{II} vs. Δ behavior for the grit blasted surfaces is

shown in Fig. 12. The plots for the fine ground and coarse ground specimens are given in Fig. 13.

5. Discussion

The constant B in Eq. (3) represents contribution of the adhesive reinforcing to the shear strength of the interface τ_{II}^{p}.

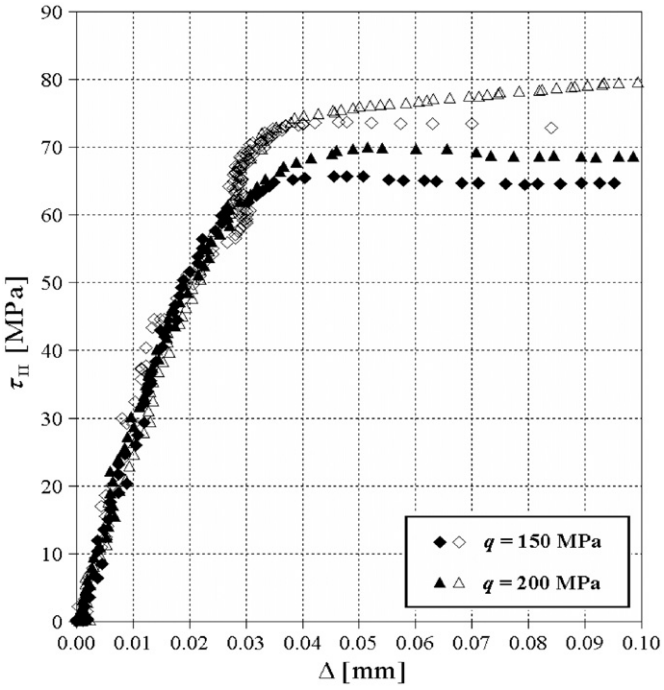

Fig. 9. Initial interface decohesion response of the coarse ground specimens. The cases $q=150$ and 200 MPa are shown.

For a specific surface condition, this value was nearly independent of q. With reference to Table 3, the highest value $B \approx 57$ MPa was obtained for the reinforced fine ground specimens. This value is approximately double the value reported by the adhesive manufacturer in Table 1. For the coarse ground and grit blasted surfaces, the respective values were 45.4 and 44.6 MPa. The slope constant A in Eq. (3) determines the rate of increase in interface shear strength with normal pressure. From Table 3, the greatest A can be found for the grit blasted surface finish. With reference to Fig. 6, the highest τ_{II}^{p} was clearly obtained for the reinforced grit blasted surface finish for the case $q=150$ MPa. It can also be seen from Fig. 6 that the rate of increase τ_{II}^{p} with q was nearly constant

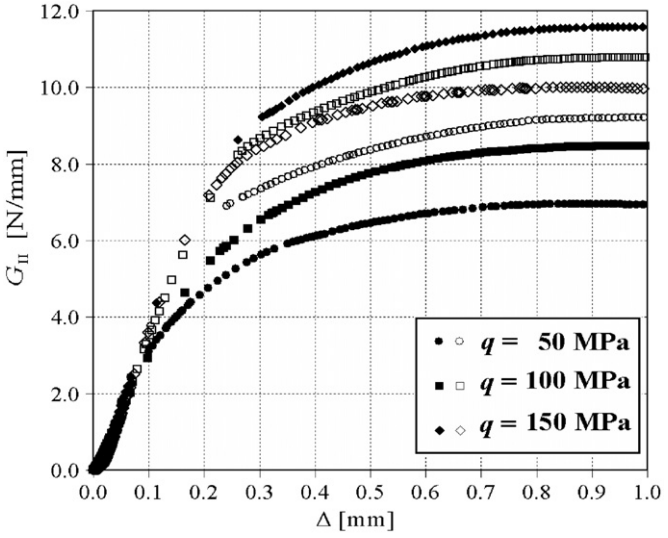

Fig. 11. R_{eff}-curves of the reinforced interfaces with the grit blasted surface finish. The filled markers correspond to the conservative result obtained from two identical tests.

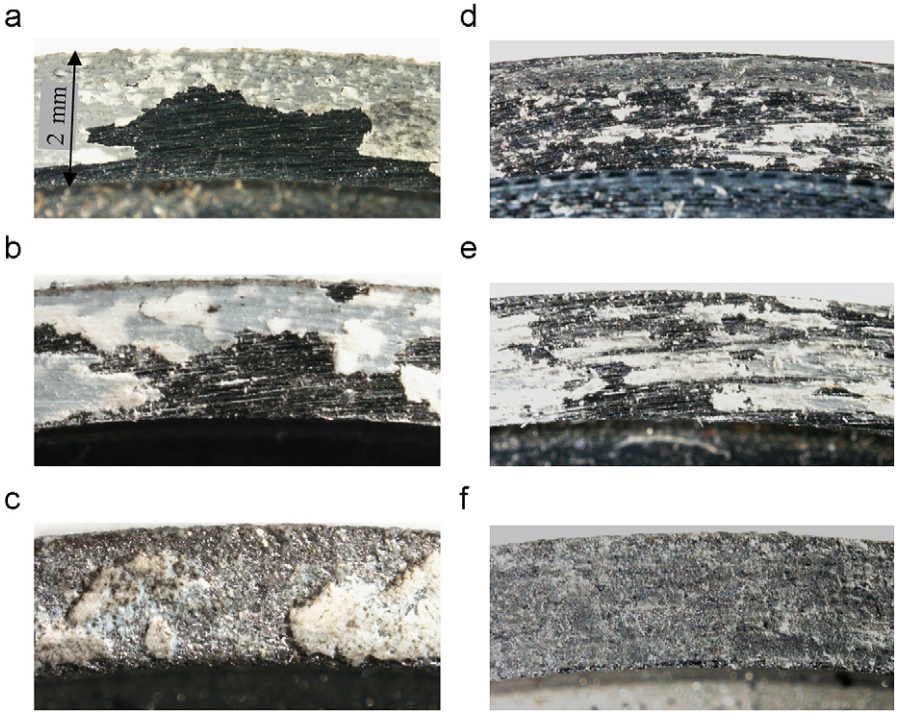

Fig. 10. Contact surfaces for $q=4$ MPa after shear fracture. (a) Fine ground, (b) coarse ground and (c) grit blasted. Damaged contact surfaces for $q=100$ MPa and $\Delta \rightarrow 3.0$ mm. (d) Fine ground, (e) coarse ground and (f) grit blasted.

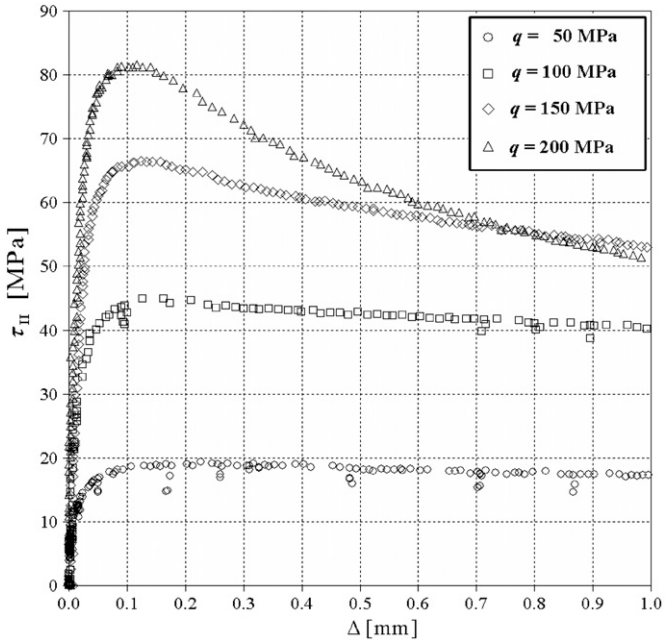

Fig. 12. Interfacial degradation responses of the non-reinforced specimens with the grit blasted contact surfaces for each q. The clearly highest interfacial damage (wear of HSS) occurs to the case with the highest clamping load, $q=200$ MPa.

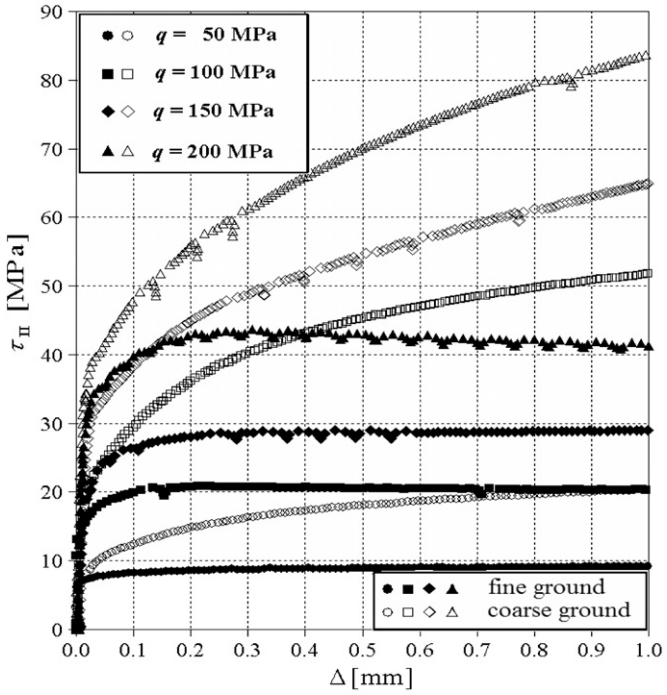

Fig. 13. Interfacial slip-response of the non-reinforced specimens with the fine and coarse ground contact surfaces for each q. The fine ground cases most closely resemble the classical Coulomb's friction law after the transient degradation vanishes. For all coarse ground cases, there clearly exists stable interface hardening.

for a particular surface finish for both bonded and non-bonded interfaces. This observation represents the superposition of adhesive strength with interface friction and corresponds to the previously published results obtained using a strong anaerobic adhesive and ground specimen interfaces [4]. In the current study, the principal of superposition accurately described the behavior of fine ground and grit blasted surfaces, but the fit was less satisfactory for coarse ground surfaces.

Fig. 9 shows the initial interface degradation response of the coarse ground specimens for the cases $q=150$ and 200 MPa. Due to the small average increase in τ_{II}^{p} for $q=200$ MPa as compared to $q=150$ MPa, the slope A for the reinforced coarse ground case differs significantly from the non-reinforced case. If the results for $q=200$ MPa are excluded, the slope $A=0.19$ is calculated, which is more consistent with the observations from other surface finishes. For the coarse ground cases, the relatively small increase in τ_{II}^{p} between $q=200$ and 150 MPa resulted, presumably, due to the subsequent unstable decohesion responses. Similar unstable fracture response was observed for grit blasted surfaces at $q=200$ MPa and these are not discussed as part of this study. The polished micro-sections in Fig. 4 show that as surface roughness increases, the contact points between interfaces become more distinct and point-like. When mode II load is applied under q, it can be expected that local multiaxial yielding occurs causing the interface to collapse. However, a more precise explanation for unstable decohesion propagation of the rougher bonded HSS interfaces involving the high pre-stress, $q \in$ [150,200] MPa, has not yet been found.

Data for the reinforced interfaces shown in Figs. 7 and 8 indicates that damage dissipation due to the combination of the normal pressure and mode II displacement occurred throughout the range of the relative displacements $\Delta^{c} \le \Delta \le 1.0$ mm. Therefore, the reinforced frictional interfaces can be assumed as fully damaged as $\Delta \to 1.0$ mm. The maximum interface traction stress t_{II}^{c} and stiffness parameter κ_{II} can be estimated from Fig. 7 for CZM of the grit blasted interface. With this information, CZM shown in Fig. 1 could be fully defined by applying the non-linear least-squares method. The response curves calculated by Eq. (7) are also shown in Fig. 7.

The individual data points in Figs. 7–9 were collected at fixed time intervals. Thus, large gaps between points indicate a very rapid increase in relative displacement at the interface. Such gaps are interpreted as representing unstable semi-brittle decohesion. A comparison of Figs. 8 and 9 shows more ductility for the coarse ground surface finish as compared to the fine ground in otherwise identical testing conditions. From Fig. 9, for $\Delta > 0.1$ mm, unstable decohesion propagation occurred especially for the tests with the highest q. Similar to the fine ground cases, the semi-brittle fracture occurred for the coarse ground specimens for both $q=50$ and 100 MPa. From Fig. 8 it can be observed, however, that the fine ground interfaces become increasingly ductile as $q \to 200$ MPa. This indicates an increasing strength contribution from friction relative to the shear strength of the adhesive. From Fig. 7, unstable decohesion response due to the semi-brittle interface fracture is observed. This is seen especially for $q=150$ MPa over the range of $0.1 \le \Delta \le 0.35$ mm where there is a sudden decrease in τ_{II} accompanied by an increase in displacement.

For all interfaces subject to small normal stress, $q=4$ MPa, the shear fracture was fully brittle. Based on Fig. 10a and b, the interfacial fracture was due to adhesive failure for both the fine and the coarse ground interfaces. In contrast, the grit blasted interface showed predominantly cohesive failure, see from Fig. 10c. Due to this differing failure mode as compared to the cases involving the greater normal pre-stress, i.e. $q \in$ [50,200] MPa, the data for $q=4$ MPa reported in Table 4 was excluded from Fig. 6 and from the regression analysis used to compute A and B. In consequence, the contribution of the reinforcing on the interface in terms of the constant B reported in Table 3 cannot directly be adapted or validated based on the values of τ_{II}^{p} from Table 4. With reference to Fig. 10d–f, which were tested with $q=100$ MPa, fully cohesive failure can be observed for all studied interface types. A comparison of Fig. 10c and f for grit blasted surfaces shows that low clamping pressure resulted in cohesive failure without noticeable damage to the HSS adherents. For high clamping pressure the surface is noticeably damaged.

Based on Fig. 11, G_{II}^{c} was attained as $\Delta \rightarrow 1.0$ mm and increased with the higher values of q. Results for the non-reinforced grit blasted specimens are shown in Fig. 12 and for the ground interface finishes in Fig. 13. The significant decrease in $\tau_{II}(1.0)$ involving the decreasing gradient can be noticed especially for the experiment with the highest q. In addition, slip hardening occurred for the non-reinforced coarse ground contact surfaces for $\Delta^{c} \leq \Delta$ for all q. This observation corresponds to the previous results published by Courtney-Pratt and Eisner [26]. Finally, the experiments on the non-reinforced specimens with the fine ground surface finish most closely resembled to the classical Coulomb's law of friction.

6. Conclusions

The influence of surface roughness and clamping load on the quasi-static shear strength of mechanically clamped steel interfaces reinforced with epoxy adhesive have been studied experimentally. Results have been assessed both in terms of computed fracture energy and interface decohesion using a linear-exponential cohesive zone model. The following conclusions can be made.

(1) For each of the three surface finishes tested, the shear strength of the bonded and non-bonded interfaces increased at a near constant rate with normal pressure. Therefore, for abraded HSS interfaces reinforced with high modulus epoxy, the principle of superposition is applicable.
(2) The contribution of the epoxy adhesive to the total shear strength of the interface varied with interface roughness. It was found to be highest for the fine ground surface finish and lowest for the grit blasted surfaces.
(3) For all values of normal pre-stress, the reinforced grit blasted interfaces resulted in the highest measured total shear strength values. Hence, surface roughness significantly influences on the quasi-static shear load carrying capacity of adhesively reinforced interfaces.
(4) The maximum observed residual slip-stresses after full decohesion, i.e. $\Delta \rightarrow 1.0$ mm, were found to be considerably higher for the grit blasted reinforced interfaces as compared to the corresponding non-bonded cases.
(5) For a relative interface displacement $\Delta = 1.0$ mm, the highest value of the critical fracture energy release rate G_{II}^{c} was attained for the grit blasted interfaces. The value of G_{II}^{c} increased with normal pressure for all surface finishes. This was due to the increased work needed to locally deform the contacting HSS surfaces.
(6) The reinforced grit blasted joint interfaces can be considered more applicable for engineering applications as compared to the other studied interface combinations and, in general, simpler joints based on either friction or bonding. This final conclusion is mainly due to the combination of the highest attained τ_{II}^{p} and the observed semi-brittle failure response.

Acknowledgments

This research work has been funded by the Technical Mechanics Graduate School in Finland. The Finnish Metals and Engineering Competence Cluster is acknowledged for providing the experimental setup. HSS material for the test specimens was provided by Ruukki.

References

[1] Mays GC, Hutchinson AR. Adhesives in civil engineering.Cambridge University Press; 1992.
[2] Albrecht P, Sahli AH. Static strength of bolted and adhesively bonded joints for steel structures. In: Johnson WS, editor. Adhesively bonded joints: testing, analysis, and design. Ann Arbor: ASTM – STP 981; 1988. p. 229–51.
[3] Gresnigt AM, Stark JWB. Design of bolted connections with injection bolts. In: Bjorhovde R, Colson A, Zandonini R, editors. Connections in steel structures III—behavior, strength and design, Proceedings of the Third International Workshop, Trento; 29–31 May 1995, p. 77–87.
[4] Dragoni E, Mauri P. Intrinsic static strength of friction interfaces augmented with anaerobic adhesives. Int J Adhes Adhes 2000;20:315–21.
[5] Dragoni E, Mauri P. Cumulative static strength of tightened joints bonded with anaerobic adhesives. Proc Inst Mech Eng Part L, J Mater—Des Appl 2002;216:9–15.
[6] Sawa T, Yoneno M, Motegi Y. Stress analysis and strength evaluation of bonded shrink fitted joints subjected to torsional loads. J Adhes Sci Technol 2001;15:23–42.
[7] Matsui K. Effects of curing conditions and test temperatures on the strength of adhesive-bonded joints. Int J Adhes Adhes 1990;10:277–84.
[8] Stewart I, Chambers A, Gordon T. The cohesive mechanical properties of a toughened epoxy adhesive as a function of cure level. Int J Adhes Adhes 2007;27:277–87.
[9] Khrulev VM. Surface roughness and rheological properties of adhesives as factors determining optimal thickness of glue line. Mech Compos Mater 1965;1:61–3.
[10] Chai H. The effects of bond thickness, rate and temperature on the deformation and fracture of structural adhesives under shear loading. Int J Fract 2004;130:497–515.
[11] Uehara K, Sakurai M. Bonding strength of adhesives and surface roughness of joined parts. J Mater Process Technol 2002;127:178–81.
[12] Shahid M, Hashim SA. Effect of surface roughness on the strength of cleavage joints. Int J Adhes Adhes 2002;22:235–44.
[13] De Bruyne NA. The measurement of the strength of adhesive and cohesive joints. In: Weiss P, editor. Adhesion and cohesion, Proceedings of the Symp Adhes Cohes, GM Res Lab, Warren Michigan, 1961: Elsevier Publishing Company; 1962, p. 47–64.
[14] Kinloch AJ. Adhesion and adhesives: science and technology. Chapman & Hall; 1987.
[15] Allix O, Ladevéze P, Corigliano A. Damage analysis of interlaminar fracture specimens. Compos Struct 1995;31:61–74.
[16] Valoroso N, Champaney L. A damage-mechanics-based approach for modelling decohesion in adhesively bonded assemblies. Eng Fract Mech 2006;73:2774–801.
[17] Pirondi A, Moroni F. Clinch-bonded and rivet-bonded hybrid joints: application of damage models for simulation of forming and failure. J Adhes Sci Technol 2009;23:1547–74.
[18] Oinonen A, Marquis G. A parametric shear damage evolution model for combined clamped and adhesively bonded interfaces. Eng Fract Mech 2011;78:163–74.
[19] De Moura MFSF. Progressive damage modelling. In: Da Silva LFM, Öchsner A, editors. Modeling of adhesively bonded joints. Berlin Heidelberg: Springer-Verlag; 2008. p. 155–82.
[20] Broek D. Elementary engineering fracture mechanics. 3rd ed. Kluwer Academic Publishers Group; 1984.
[21] Bao G, Suo Z. Remarks on crack-bridging concepts. Appl Mech Rev 1992;45:355–66.
[22] Nairn JA. Analytical and numerical modeling of R curves for cracks with bridging zones. Int J Fract 2009;155:167–81.
[23] Rice JR. A Path independent integral and the approximate analysis of strain concentration by notches and cracks. J Appl Mech 1968;35:379–86.
[24] 3M United Kingdom PLC. Scotch-Weld™ EPX™ Epoxy adhesive DP760 product data sheet; 2001.
[25] The MathWorks. Curve fitting toolbox—parametric fitting. Accessed 30 September 2010. Available from: ⟨http://www.mathworks.com/access/helpdesk/help/toolbox/curvefit/⟩.
[26] Courtney-Pratt JS, Eisner E. The effect of a tangential force on the contact of metallic bodies. Proc Roy Soc London Ser A Math Phys Sci 1957;238:529–50.